THE ARCHIVE OF MECHANICAL ENGINEERING

VOL. LVI 2009 Number 2

DOI: 10.24425/ame.2009.132091

Key words: transonic wind tunnel, test section wall interferences, high airfoil angle of attack, numerical simulation

WITOLD C. SELEROWICZ *

PREDICTION OF TRANSONIC WIND TUNNEL TEST SECTION GEOMETRY – A NUMERICAL STUDY

The paper presents numerical simulations related to the problem of how to obtain correct results in transonic wind tunnel during tests at high airfoil angles of attack. At this flow conditions, significant pressure losses appear in the test section, what leads to significant errors in measured data. Regarding the possible ways of tunnel reconstruction, we examined three different possibilities of changing the test section configurations: an increase of the test section height, displacement of the airfoil below the tunnel centreline and, finally, introduction of divergent test section walls. It was shown that neither the use of higher test section, nor the change of the airfoil location, gives any significant improvement in reference to the existing tunnel configuration. Only after divergent test section walls were introduced, the distributions of pressure coefficient became well consistent with their expected values.

1. Introduction

1.1. The ITLiMS transonic wind tunnel

The transonic wind tunnel at the Department of Aerodynamics is a relatively small installation designed to do experiments at transonic speeds. The overview and arrangement of its test section are shown in Fig. 1 and Fig. 2. The working medium (air) is sucked from the ambient or from special elastic reservoir of 50 m^3 volume (not visible in Fig. 1) into a vacuum tank (6) of a volume of 150 m^3 through the tunnel test section. The test cycle begins with opening the cut-off valve (5) and goes on for about $0.1 \div 1$ s. Afterwards, the cut-off valve closes automatically. This time is sufficient to achieve a steady flow conditions in the test section, and to store all measured data. It is also long enough to perform flow visualization. The velocity of the mean flow is

* *Warsaw University of Technology Institute of Aeronautics and Applied Mechanics; ul. Nowowiejska 24, 00-665 Warsaw, Poland; E-mail: seler@meil.pw.edu.pl*

precisely regulated with the control valve (7). The Mach number of the main flow can achieve during the experiments a value up to 0.8.

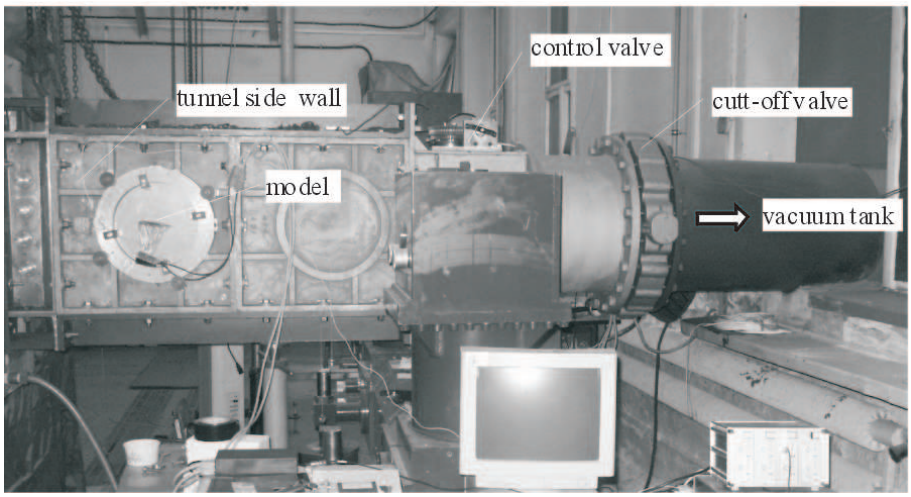

Fig. 1. View of the transonic wind tunnel

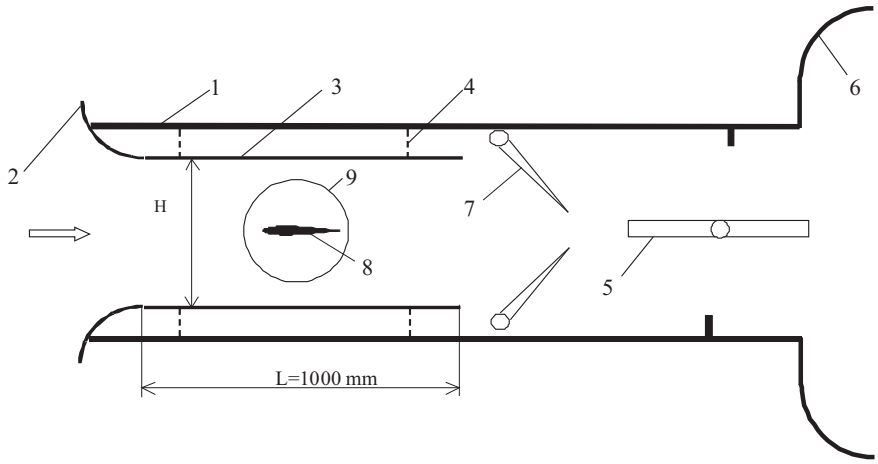

Fig. 2. Scheme of arrangement of transonic wind tunnel test section: 1 – tunnel wall, 2 – intake wall, 3 – test section wall, 4 – adjusting screw, 5 – cut-off valve, 6 – vacuum tank, 7 – control valve, 8 – NACA 0012 airfoil, 9 – glass window used in flow visualisation

The sidewalls of the tunnel consist of massive aluminium plates, with dimensions of 600×600 mm, mounted to the top and bottom tunnel walls (1). Due to this construction, the test section width B remains constant and equal to 100 mm.

Unlike the sidewalls, the inner top and bottom walls of the test section (3) are mounted to the tunnel walls (1) by means of the adjusting screws (4), so that the height of the test section can vary. During the tests at low airfoil angle of attack it typically equals 440 mm (the test cross-section area A = 0.044 m^2). This size of the test section makes it possible to perform up to 10 tests before the vacuum tank must be evacuated again.

The model (airfoil), which is placed in the centre of the test section, has usually the chord length of 120 mm and the span of 100 mm. Its interior is specially prepared to allow for steady and unsteady pressure measurements. In the first case, a series of 32 holes with diameter of 0.4 mm are drilled in the centreline of the model surface. Each hole is linked to a 2 mm pipe placed inside the model. All pipes are connected with a special multi-channel pressure scanner (located outside the test section) by means of elastic pressure conduits.

Contrary to the previous case, to measure unsteady pressures one uses 16-miniature piezoresistive transducer mounted directly inside the model. Each of them has a diameter of 2.3 mm and a length of 15 mm. Their size determines the overall minimal model dimensions.

1.2. Test section walls – model interferences

It is well known that during wind tunnel tests various undesirable interactions between the model and the test section walls occur. The model body disturbs the flow in a relatively small test section, so that it is completely different compared to the free-flow (model blockage). This effect depends on the model size as well the lift on the model (Pankhurst and Holder [1], Pope [2]). The proximity of walls leads to additional effects such as increased velocity in the region of maximum model thickness and in the region of decreased pressure. This disturbed flow field can cause changes in the shock position on the model, especially in the case of transonic airfoil flow. The boundary layer on the test section walls generates an acceleration of the flow that leads to additional drag on the model (Barlow [3]). As a consequence, the obtained data must be corrected, or the flow in the test section must be corrected during the test (Ewald [4]).

To minimize the wall interferences, two general methods can be used: the test section with ventilated walls and the test section with adaptive walls.

Ventilation of the test section can be realized by means of slots and perforation (Goethert [5]). In the case of 2d transonic wind tunnel at the ITLiMS, this method is applied on the top and bottom test section walls in the form of 10 parallel slots 2 mm wide and 1 m long. Because the test section dimensions are (400×100 mm), only 18.5% of the whole test section

area can be ventilated in this way. This is sufficient at thin airfoils and small angles of attack, but in the case of high blockage (thick airfoils and high angles of attack) it could not work effectively.

The second method, called the adaptive wall test section technology (AWTS), has been applied in many installations. An extensive review of this problem with various examples is presented by Ganzer [6], Sears [7], Wolf [8] and Meyer and Nitsche [9]. The use of this method in the case of 2d tunnels needs flexible walls introduced on the top and bottom of the test section. In consequence, the tunnel height in the airfoil neighbourhood increases (Romberg [10]). An advantage of this method seems to be the possibility of independent arrangement of the bottom and upper test section walls. This is technically rather complicated and, in addition, both contours must be preliminarily defined by calculations. Amecke [11] has shown that this can be realized in a few steps. A further development of this method consists in the idea of self-correcting wind tunnel presented by Sears [12].

The configuration of the test section described above is satisfactory for experiments at small airfoil angles of attack. However, in some experiments this angle must be significantly greater. This occurs for example when examining the buffet phenomenon (airfoil angle of attack of about 8 degree), or when the flow is fully separated from the airfoil surface (what happens at airfoil angle of attack above 10 degree). In such cases, the flow in the test section is strongly disturbed by the model, and the wake is extremely high (model and wake blockage). All of this leads to abnormal pressure losses along the test section and in consequence to great errors in measured data. On the other hand, some of such phenomena must be still investigated experimentally, because of lack of software for numerical examination.

The situation described above suggests that the tunnel test section should be modified. To perform such modification, two steps are necessary:
Step 1. To perform a numerical study in order to obtain proper configuration of the test section.
Step 2. To introduce changes and to examine the new test section in experimental tests.

In this paper, only the first step, namely the numerical study, is presented. All simulations has been perform using commercial CFD code Fluent.

2. Numerical simulations

The general view of the modelled volume and the applied boundary conditions is shown in Fig. 3a. Due to the tunnel symmetry, the flow in its test section was modelled only in a half of it. At the intake of the test section, a "pressure-inlet" condition was assumed, whereas at its end a "pressure-outlet"

boundary condition was adopted. Both the upper and bottom test section walls, as well as the tunnel sidewall, were modelled as the "walls". In the tunnel symmetry plane, the "symmetry" boundary condition was assumed.

To make changing the airfoil angle of attack possible, the whole volume was divided into two parts. The first one (Fig. 3b) included the NACA 0012 airfoil, and has a fine mesh with boundary layer around the airfoil, whereas the second one (Fig. 3c) contained the remaining part of the tunnel with much thinner mesh. Both volumes were joined together using an interface.

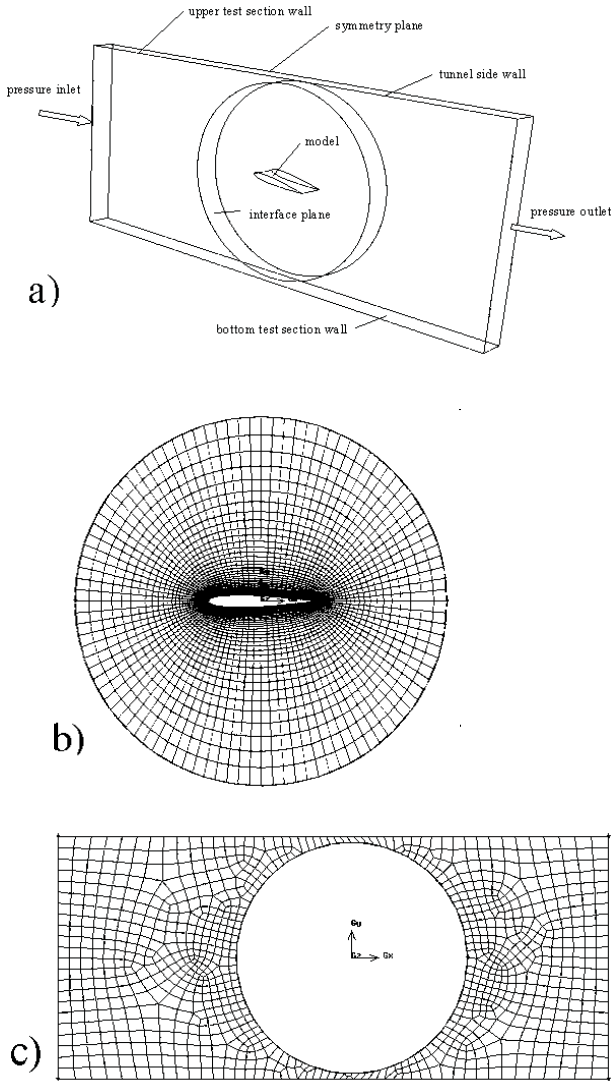

Fig. 3. Meshes and boundary conditions used for calculations in the case of tunnel flow: a) boundary conditions, b) mesh around the model, c) mesh in the tunnel

Considering high Mach numbers of the flow, a model of ideal-gas was assumed. Because the Reynolds number, based on the airfoil chord length and flow velocity, was about $2 \cdot 10^6$, a turbulent flow conditions had to be assumed. Due to the possibility of the presence of shock waves, a Spalart-Almaras scheme of turbulence was applied.

To facilitate the comparison between the calculated results and characteristics of the same NACA 0012 airfoil in the case of free flow, some other simulations for a 2d model were performed. The mesh used for these calculations is presented in Fig. 4a, whereas in Fig. 4b boundary conditions are shown. On the external flow boundaries, the "far-field" boundary conditions with constant flow parameters were used. For further comparison with the flow in the tunnel, one additionally defined two pairs of virtual lines. Each of these lines has a length of 1 m (identical as the length of the test section walls), and was placed at the same position in reference to the airfoil as the upper and bottom walls of the test section. The distance between the lines was equal to 440 mm in the first case (reference configuration) and 540 mm in the case of enlarged cross-section.

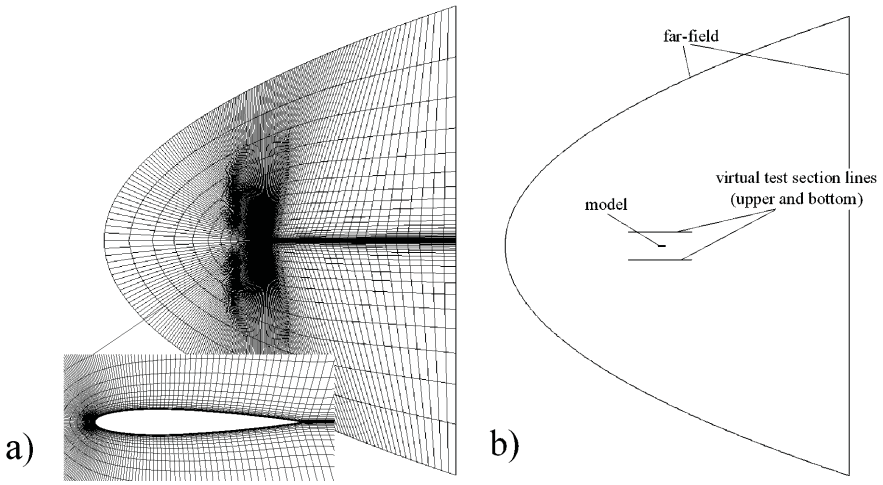

Fig. 4. Mesh (a) and boundary conditions (b) used for calculations in the case of free flow

All numerical simulations presented in this study were performed for a reference Mach number equal 0.7 and three values of the airfoil angle of attack, namely $\alpha = 4°$, $8°$ and $12°$.

3. Flow in test section with solid parallel walls

First of all, the numerical calculation were performed for transonic flow over a NACA 0012 airfoil placed in the centre of the test section of 440 mm

height with solid parallel walls. The results are presented in form of pressure coefficient distribution on both upper (suction) and bottom (pressure) airfoil surface. The C_p values were calculated according to the formula

$$C_p = \frac{p - p_{ref}}{q_{ref}} = \frac{2(\frac{p}{p_{ref}} - 1)}{\gamma M_{ref}^2} \tag{1}$$

where:

p – pressure,

p_{ref} – reference pressure,

$q_{ref} = \rho_{ref} V_{ref}^2/2$ – reference dynamic pressure,

M_{ref} – reference Mach number,

γ – ratio of specific heats.

When the flow in the tunnel is considered, the reference values pertained to those at the inlet of the test section, whereas in case of the free flow – they referred to the values at the far-field boundary. In all cases, longitudinal positions on the airfoil surface were normalized in reference to the chord length c.

Fig. 5 shows the results calculated for the tunnel flow compared with those for the free flow at $M_{ref} = 0.7$. As it can be seen in this plots, for the considered angles of attack ($\alpha = 4^\circ, 8^\circ$ and 12°) one can notice distinct differences between C_p values in the case of tunnel and free flow, especially in the rear part of the airfoil. At $\alpha = 4^\circ$ (Fig. 5a) the C_p values on the upper (suction) airfoil surface exhibit a good agreement only in the first part, whereas in the remaining part both distributions distinctly differ. However, it can be seen that the shock position, which is manifested by rapid C_p increase, appears approximately at the same x/c value. Unlike to what is observed on the upper surface, C_p, the distributions on the bottom (pressure) airfoil side differ in the whole x/c range. The values of C_p at the trailing edge (x/c = 1) become negative value in case of tunnel flow and positive in case of the free flow.

Similar behaviour can be observed at the angle of attack of $\alpha = 8^\circ$ (Fig. 5b). Although the differences in the shock location (x/c) appear to be small, behind the shock C_p both distributions distinctly differ. In the case of free flow (lines without symbols) the pressure on the upper surface still increases, whereas in case of tunnel flow (lines with symbols) a range of nearly constant C_p can be observed. At the trailing edge (x/c = 1), the difference between C_p for tunnel and free flow reaches a value of 0.6.

Much greater differences, especially on the upper airfoil surface, can be noted at the angle of attack $\alpha = 12^\circ$ (Fig. 5c). In the case of free flow (lines without symbols), we can observe a full separation of the flow already

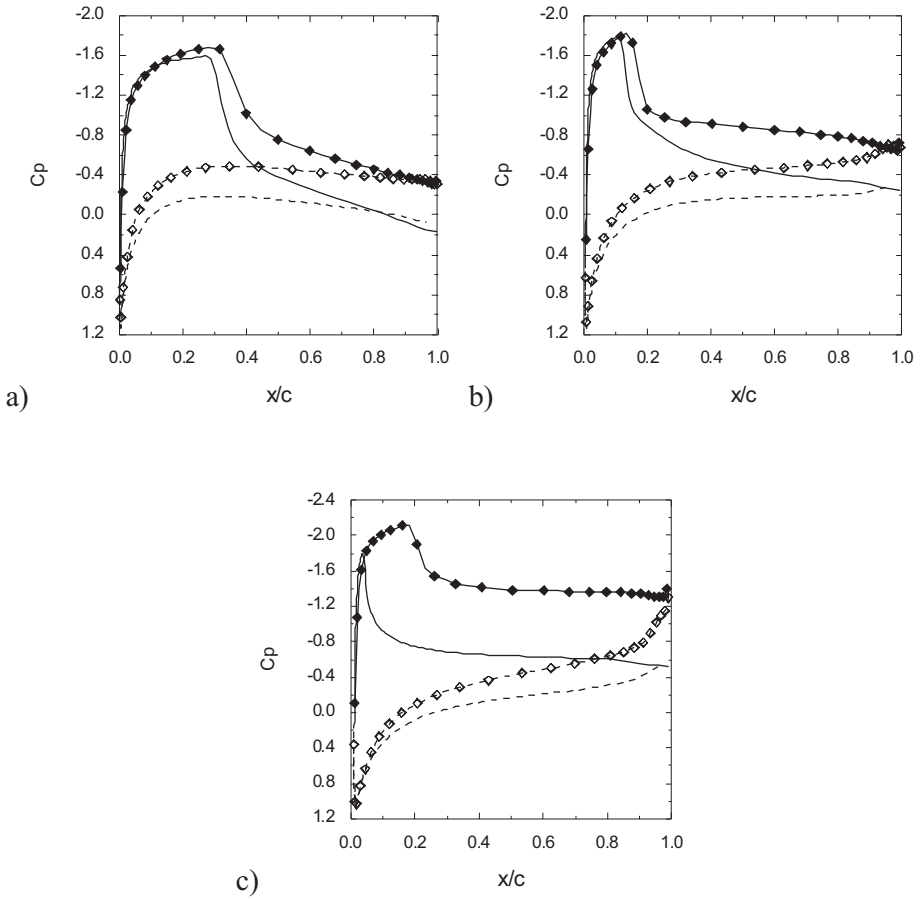

Fig. 5. Comparison of data calculated for the cases of tunnel flow (test section high H = 440 mm, lines with symbols) and free flow (without symbols). Distribution of pressure coefficient C_p on upper (continuous lines) and bottom (dashed lines) airfoil surface. M_{ref} = 0.7. Airfoil angle of attack: a) $\alpha = 4°$, b) $\alpha = 8°$, c) $\alpha = 12°$

at x/c = 0.15. For the case in which the model is placed in the tunnel, a continuous acceleration of the flow in this airfoil part can be seen. The flow becomes supersonic with a shock wave located at x/c = 0.18. Behind the shock, C_p value increases slightly from −1.6 up to −1.5. At the trailing edge (x/c = 1), the difference in C_p values between tunnel and free flow cases reaches a value of 1.5.

These observations are additionally confirmed by the contours of the Mach number shown in Fig. 6. The results for tunnel flow are shown in the left column, whereas in the right one – those for the free flow. As it can be seen in Figs. 6a and 6b, at the angle of attack $\alpha = 4°$ one can note only

small differences. The M = 1 line, which marks the supersonic flow region, is similar in both cases. In the case of tunnel flow, the separation region behind the shock is visible, whereas in the case of free flow the flow it seems to be attached behind the shock.

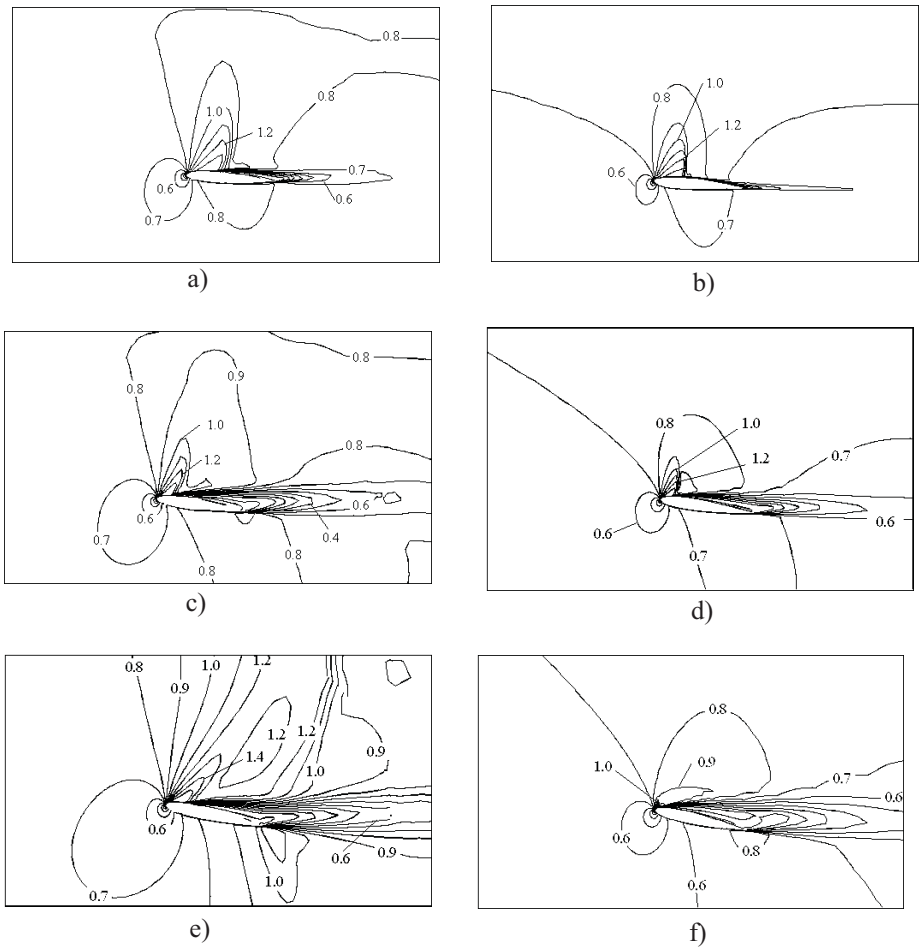

Fig. 6. Contours of Mach number calculated for tunnel flow (test section high H = 440 mm, left column) and free flow (right column). M_{ref} = 0.70. Airfoil angle of attack: a) and b) $\alpha = 4°$; c) and d) $\alpha = 8°$; e) and f) $\alpha = 12°$

The contours of Mach number plotted for the angle of attack $\alpha = 8°$ (Fig. 6c and 6d) exhibit higher differences. In the case of tunnel flow (left column), the region of $M > 1$ is wider, and so is the separation region.

At the angle of attack $\alpha = 12°$, the calculated contours of Mach number are, for both considered cases, distinctly different, especially on the upper airfoil side. The results presented for the flow in the tunnel (Fig. 6e) show that on the suction side there appears a big supersonic flow region with the

Mach number exceeding a value of M = 1.5. Just behind the shock, the flow separates from the airfoil. In the case of free flow (Fig. 6f), this supersonic region is not visible at all. Instead, the flow separates just from the edge of attack, and later it remains separated.

All the differences described above are due to the fact that, in the case of tunnel flow, the airfoil (mounted at high angle of attack) is a source of strong flow disturbances. This leads to high pressure losses in the case of tunnel flow. In consequence, pressure distributions along the tunnel test section walls differ significantly from pressure distributions along the virtual line in the case of free flow. As mentioned in section 2, both lines have the same location in relation to the airfoil as the test section walls.

Pressure distributions on both test section walls for all the considered angles of attack ($\alpha = 4^\circ, 8^\circ$ and 12°) are shown in Fig. 7a, 7b and 7c (because the flow in the tunnel is three-dimensional, only the distributions in the symmetry plane are shown). They are compared with the pressure values on virtual lines in the case of free flow, which represent test section walls. All the pressures are brought to a non-dimensional form with the use of a reference pressure (the far-field boundary pressure for free flow and the value on test section inlet for tunnel flow). The longitudinal wall distance x is also made non-dimensional by the use of the test section length L. In all plots shown in Fig. 7, one can observe a distinct decrease of pressure in the central part (x/L≈0.5), which corresponds with the position of the airfoil.

As it can be seen in all plots, the values of wall pressure distribution calculated for the case of tunnel flow differ distinctly from similar values calculated for an undisturbed (free) flow. Generally, in the case of free flow, the pressure at the end of the virtual wall is nearly the same as the pressure at its beginning. In contrast, in the case of tunnel flow, at the end of the test section pressures are visibly lower then those at the inlet. At the angle of attack $\alpha = 4^\circ$ (Fig. 7a), the pressure at the end of test section is 10% lower then at the beginning (on both upper and bottom wall), whereas in the case of free flow the pressure at the end of the virtual line is nearly the same as that at its beginning. In the central part of the wall (the position of the airfoil) the pressures also differ from those for the case of free flow.

At the angle of attack $\alpha = 8^\circ$ (Fig. 7b), one can see a similar character of changes on upper and bottom walls. As before, at the end of the test section (x/L = 1) the pressures calculated for the case of tunnel flow are by about 10% lower then at its beginning. In the case of free flow, this difference is negligible.

A completely different behaviour can be observed at $\alpha = 12^\circ$ (Fig. 7c). As before, at the end of the test section, pressures decrease up to the value of 0.8, whereas in the case of free flow no differences can be seen. On the

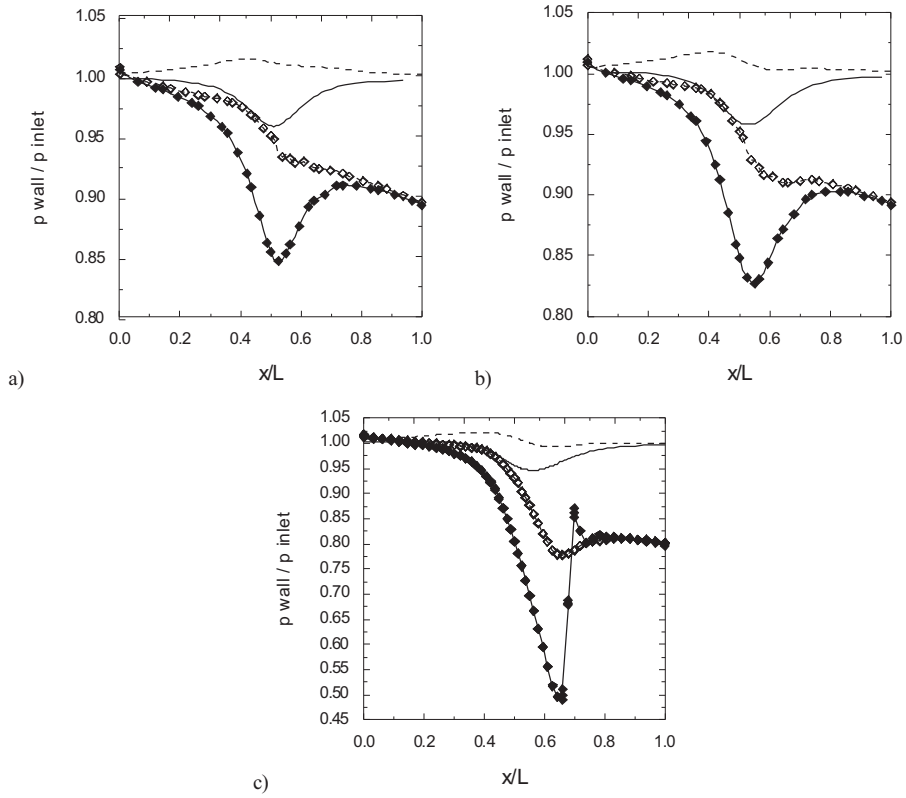

Fig. 7. Pressure distribution along the test section walls (test section high H = 440 mm, lines with symbols) and imaginary lines in free flow (without symbols). Upper wall – continuous lines, bottom – dashed lines. M_{ref} = 0.7. Airfoil angle of attack: a) $\alpha = 4^\circ$, b) $\alpha = 8^\circ$, c) $\alpha = 12^\circ$

bottom side of the test section wall, the pressure reaches a minimal value of 0.78 (at x/L = 0.65), whereas in the case of free flow, the pressure has a different distribution. Unlike to that on the bottom wall, the upper wall pressure decreases up to the value of 0.5 at x/L = 0.65, and dramatically differs from the values for the free flow (in the case of free flow, the minimum value is 0.95 only, and is observed at x/L = 0.55). This situation is due to the existence of the supersonic flow region, visible in Fig. 6e.

All the pressure distributions discussed above indicate that the model placed at the high angle of attack causes an additional choking effect. In consequence, all measurements taken in the tunnel must be considered unbelievable and often unphysical.

To improve this situation, one can possibly apply the following methods:

a) To suck off the boundary layer on all test section walls. This does not seem to be effective, because the "chocking effect" can not be eliminated in this way.

b) To increase the test section dimensions. This can, first of all, diminish the "choking effect". However, it follows from the tunnel construction that this increase can only be achieved by an increase of the test section height. Because the maximal height of the test section can be 540 mm, the effective increase is 23% only. An additional step seems to be placing the model bellow the test section centerline. It is evident that, because of the tunnel construction, the model can be lowered by about 40 mm only. The results obtained during numerical simulation for all these cases will be presented in chapter 4.
c) To introduce divergent sidewalls of the test section. Because of the tunnel construction it is evident that it can be done with the top and bottom test section walls. This problem will be the subject of discussion in chapter 5.

4. Flow in enlarged test section

The results of numerical simulations presented in this chapter were obtained for two test section configurations:
1) test section with enlarged (up to 540 mm) parallel upper and bottom walls and with the model placed in the centreline of the test section, and
2) test section as above but with the model placed 40 mm below the tunnel centreline.

Pressure distributions on both, upper and bottom, test section walls are presented in Fig. 8. The results of calculations were compared with pressure distributions along virtual lines in free flow, which were placed at a distance of 540 mm from each other. The pressure distributions in the existing test section (H = 440 mm) are also presented.

As it can generally be seen from Fig. 8, the increase of the test section height up to 540 mm does not give any significant improvement. At the angle of attack $\alpha = 4^\circ$ (Fig. 8a), at the end of the test section the pressure reaches a value of 0.93; the same value equals 0. 90 in the case of H = 440 mm. At the angle of attack $\alpha = 8^\circ$ (Fig. 8b) these values are 0.92 and 0.89, respectively, what means a 3% difference. An increase of the test section height gives an improvement only at the angle of attack $\alpha = 12^\circ$ (Fig. 8c). First of all, the wide range of low pressures (which denotes the supersonic flow region) can not be seen now. The pressure at the end of the test section (x/L=1) is now 18% lower in comparison with 20% in the case of H = 440 mm. The presented calculations shown that, at the end of the test section wall, the pressures are higher (what indicates lower flow losses) but they are still much lower than those in the case of free flow.

It is also worth mentioning that the displacement of the model does not have any significant influence on the wall pressure distribution, especially on

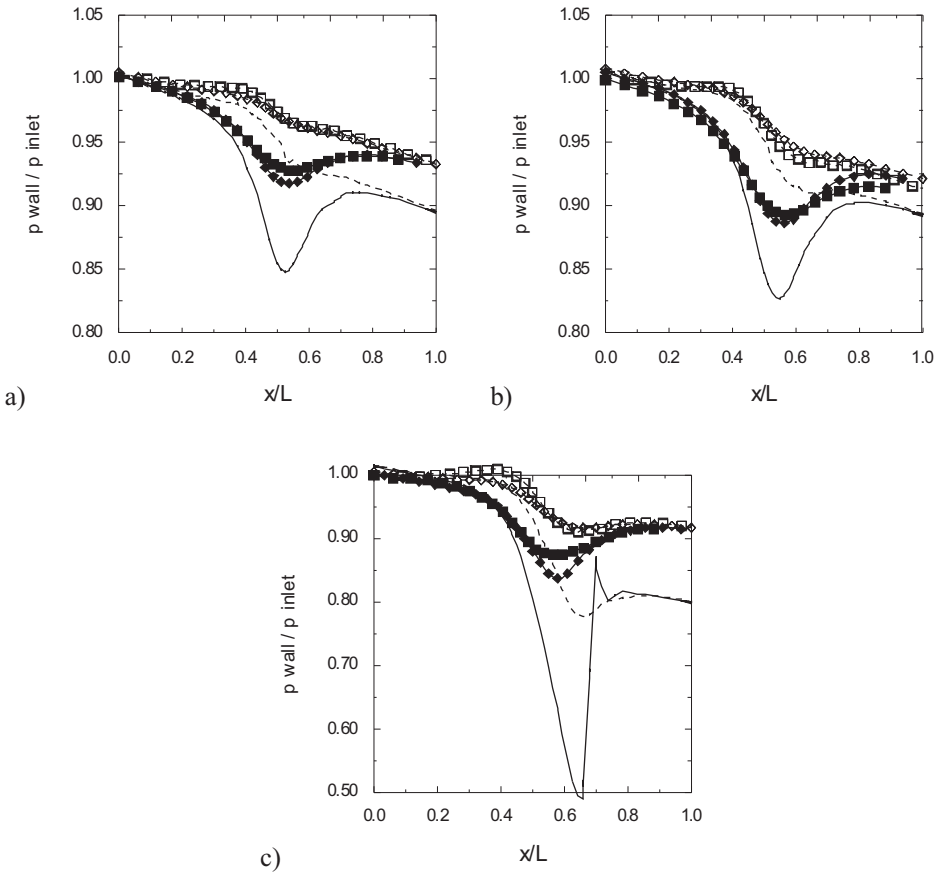

Fig. 8. Comparison of pressure distribution along upper and bottom test section walls, calculated for the case of tunnel flow with increased (H = 540 mm) and existing (H = 440 mm – lines without symbols) test section. Model located in the tunnel centreline (filled and open rectangles) and 40 mm below the centreline (filled and open aslant rectangles). M_{ref} = 0.7, airfoil angle of attack: a) $\alpha = 4^\circ$, b) $\alpha = 8^\circ$, c) $\alpha = 12^\circ$

the bottom wall at $\alpha = 4^\circ$ and $\alpha = 8^\circ$. Small differences can be observed at $\alpha = 12^\circ$ only. Irrespectively of the model location (on the centreline or below it), the calculations show the same wall pressures at the outflow from the test section.

The distributions of pressure coefficient C_p for both considered cases compared with C_p distributions for the case of free flow are shown in Fig. 9. As one can see in these plots, the increase of the test section does not lead to the expected distributions. One can see the same differences in C_p distribution as in the case of test section height of H = 440 mm (see Figs. 5a and 5b).

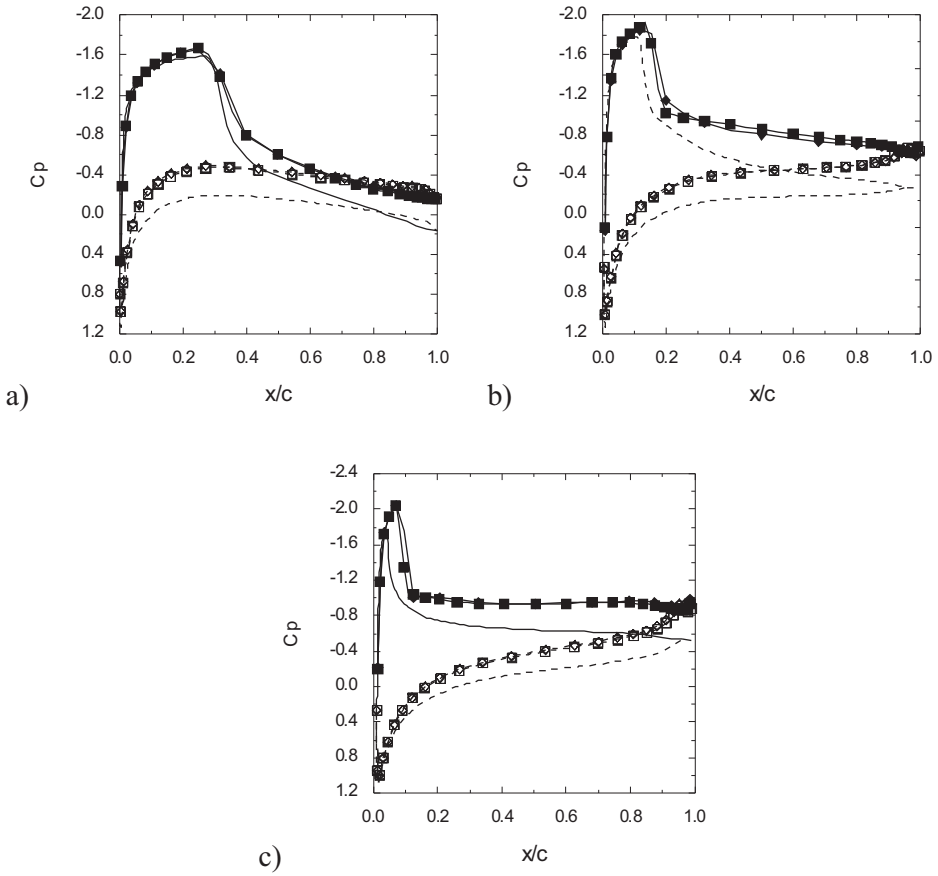

Fig. 9. Comparison of pressure coefficient distribution along upper (continuous lines) and bottom (dashed lines) airfoil surface. M_{ref} = 0.7. Calculations performed for tunnel flow (test section high H = 540 mm, lines with symbols) and free flow (without symbols). Model located in the tunnel centreline (filled and open rectangles) and 40 mm below the centreline (filled and open aslant rectangles). Airfoil angle of attack: a) $\alpha = 4^\circ$, b) $\alpha = 8^\circ$, c) $\alpha = 12^\circ$

5. Test section with divergent walls

The last considered test section modification, presented in this paper, is the test section with divergent walls.

The angle of wall divergence β was chosen individually for each value of airfoil angle of attack. After one simulation, the value of β was changed and simulations were repeated until the pressure at the end of the test section was less than 5% different from the expected value (in free flow). In this way, the values of wall divergence for any angle of attack were determined. They were $\beta = 1.01^\circ$ for $\alpha = 4^\circ$, $\beta = 1.01^\circ$ for $\alpha = 8^\circ$ and $\beta = 1.2^\circ$ for $\alpha = 12^\circ$.

The calculated wall pressures distributions are shown in Fig. 10. In contrast to the case of parallel test section walls (see Fig. 7), the pressures at the and of test section are now slightly higher then at the inlet, but the difference is only about 2.5%. This value seems to be fully acceptable.

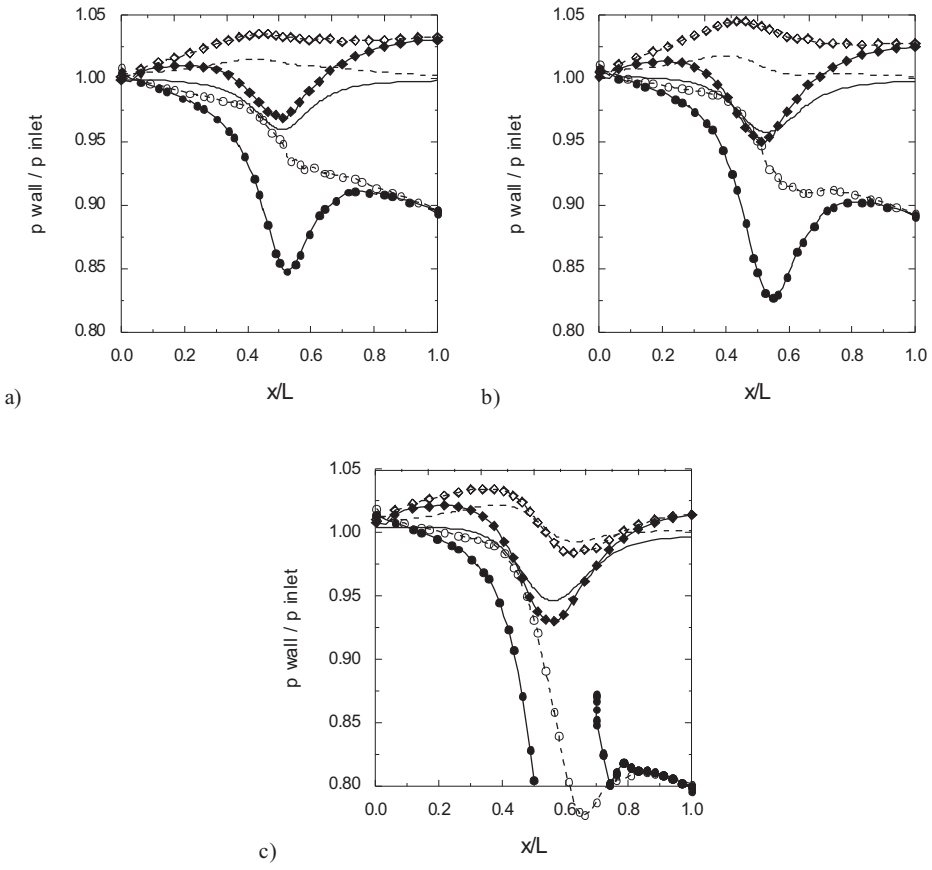

Fig. 10. Pressure distribution along upper (continuous lines) and bottom (dashed lines) test section wall. Comparison of calculations for tunnel with parallel walls (open and filled circles), tunnel with divergent walls (open and filled rectangles) and free flow (without symbols). Initial test section height H = 440 mm, M_{ref} = 0.7. Airfoil angle of attack α and test section divergence β are: a) $\alpha = 4°, \beta = 1.01°$, b) $\alpha = 8°, \beta = 1.01°$, c) $\alpha = 12°, \beta = 1.2°$

Similarly, one can notice a good agreement in C_p distribution (Fig. 11), especially on the bottom airfoil surface. On the trailing edge (x/c = 1), the values of C_p are the same, especially at 4 and 12°. Some small differences can be observed on the airfoil upper surface only. This leads, at $\alpha = 4°$ (Fig. 11a), to a small difference in shock position ($x_{shock}/c = 0.2$ in the case of test section with divergent walls, compared to $x_{shock}/c = 0.3$ in case of free

flow). Behind the shock, a fully attached flow can be observed in both cases. In the rear part of the airfoil, the distributions of C_p seem be identical.

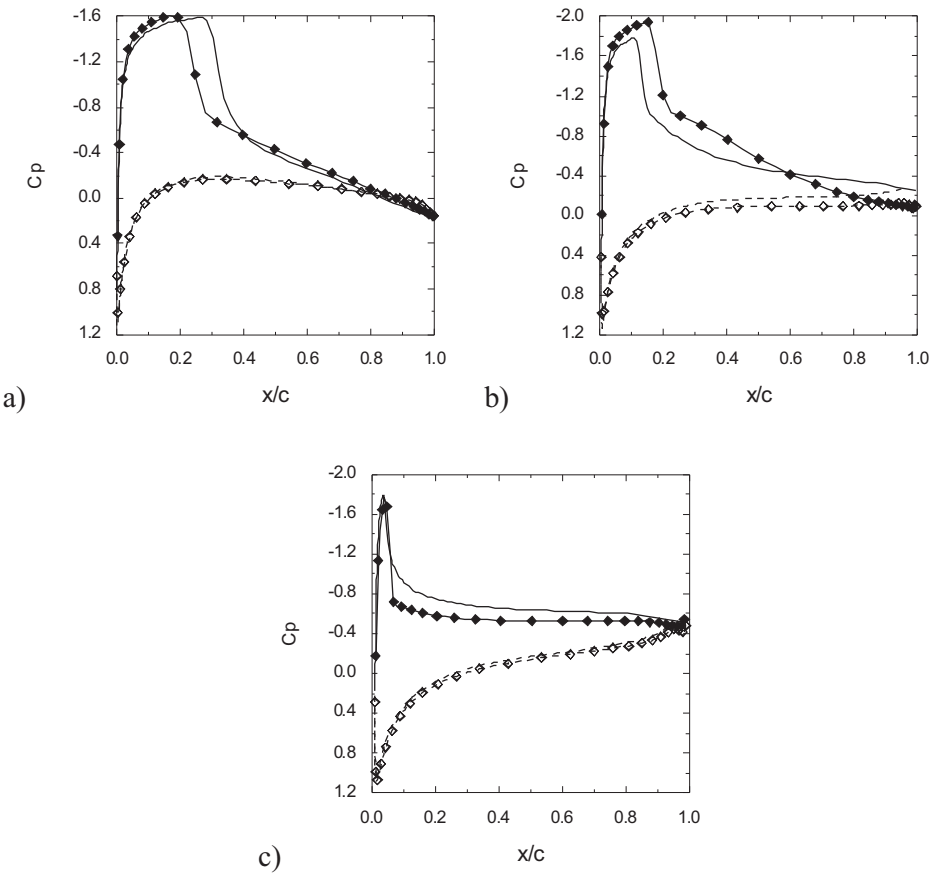

Fig. 11. Distribution of pressure coefficient C_p along upper (continuous lines) and bottom (dashed lines) airfoil surface. M_{ref} = 0.7. Comparison of calculations in the cases of tunnel flow (divergent test section, initial high H = 440 mm, lines with symbols) and free flow (without symbols). Airfoil angle of attack α and angle of test section divergence β are:
a) $\alpha = 4°, \beta = 1.01°$, b) $\alpha = 8°, \beta = 1.01°$, c) $\alpha = 12°, \beta = 1.2°$

At $\alpha = 8°$ (Fig. 11b), small differences in shock location are still visible ($x_{shock}/c = 0.15$ in the case of divergent tunnel and $x_{shock}/c = 0.2$ in the case of free flow).

The simulations at $\alpha = 12°$ (Fig. 11c) demonstrate that the flow separates from the airfoil at the same position (x/c = 0.05) in the cases of tunnel and free flow. In the rear part of the airfoil, C_p distribution demonstrates that the flow on the upper airfoil side remains separated. On the trailing edge (x/c = 1), C_p values are the same in both cases.

6. Conclusions

In relatively small tunnel test section, undesirable effects can be observed at transonic speeds. When airfoil angles of attack are high, the flow is choked by the airfoil. This results in excessive high pressure losses. In consequence, at the end of the test section, the pressure is up to 20% lower than in the inlet plane. Such behaviour leads to strong differences in C_p distribution on both airfoil surfaces. Unexpected unphysical phenomena can also take place. For these reasons, the results of measurements could be unreliable.

The numerical simulation presented in this study concentrates on the possibility of diminishing this effect. This was done by introducing changes in the section configurations. Three of such possibilities were examined: increasing the test section height, placing the airfoil below the tunnel centreline, and using the test section with divergent walls.

All the data were compared with the results of similar calculations performed for the case of free flow. The presented results allow us to draw the following conclusions:

1. In the case of enlarged test section height (from the existing 440 mm up to 540 mm), there haven't been any significant improvement in the results. Similar behaviour was observed even in the case when the airfoil was additionally displaced to the position of 40 mm below the test section centreline.
2. As soon as the test section walls become divergent, satisfactory results could be obtained. The differences in the wall pressure at the end of the test section became smaller then 5% in comparison to the free flow (3% at $\alpha = 4^\circ$; 2.5% at $\alpha = 8^\circ$ and 2% at $\alpha = 12^\circ$). In consequence, one can observe nearly the same pressure coefficient distributions as in the case of free flow on both airfoil surfaces.

An inconvenience of the presented method is that the angle of wall divergence must be determined individually, depending on airfoil angle of attack (and the flow Mach number also). This can be difficult to realise. Nevertheless, in the considered test, this should be done before experimental investigations are performed.

Manuscript received by Editorial Board, February 25, 2009;
final version, August 27, 2009.

REFERENCES

[1] Pankhurst R.C., Holder D.W.: Wind-tunnel technique. 1st ed. London: Sir Isaac Pitman & Sons Ltd, 1952.
[2] Pope A.: Wind-tunnel testing. 2nd ed. New York, Wiley, 1954.

[3] Barlow J.B., Rae Jr W.H., Pope A.: Low-speed wind tunnel testing. 3rd ed. New York, Wiley, 1999.
[4] Ewald B.R.F. (editor):Wind tunnel wall corrections. AGARDograph-336, 1999.
[5] Goethert B.H.: Transonic wind tunnel testing. New York, Pergamon Press, 1961.
[6] Ganzer U.: A review of adaptive wall wind tunnels. Progress in Aerospace Sciences, Vol. 22, pp. 81-111, 1985.
[7] Sears W.R., Erikson J.C.: Adaptive wind tunnels. Annual Review of Fluid Mechanics, Vol. 20, pp. 17-34, 1988.
[8] Wolf S.W.D.: Adaptive wall technology for improved wind tunnel testing techniques – a review, Progress in Aerospace Sciences, Vol. 31, pp. 85-136, 1995.
[9] Meyer O., Nitsche W.: Update on progress in adaptive wind tunnel technology, Progress in Aerospace Sciences, Vol. 40, pp. 119-141, 2004.
[10] Romberg H.-J.: Two-dimensional wall adaption in the transonic windtunnel of the AIA, Experiments in Fluids, Vol. 9, No 3, pp. 177-180, 1990.
[11] Amecke J.: Direkte Berechnung von Wandinterferenzen und Wandadaption bei zweidimentionaler Strömg in Windkanälen mit geschlossenen Wänden. DFVLR-FB 85-62.
[12] Sears W.R.: Self correcting wind tunnels, Aeronautical Journal, Vol. 78, pp. 80-89, 1973.

Wyznaczanie geometrii przestrzeni pomiarowej tunelu transonicznego – studium numeryczne

S t r e s z c z e n i e

W pracy przedstawiono studium numeryczne dotyczące wstępnego definiowania ustawienia przestrzeni pomiarowej tunelu transonicznego podczas pomiarów profili lotniczych ustawionych pod bardzo dużymi kątami natarcia. W takich przypadkach duże straty ciśnienia w tunelu, spowodowane dławieniem przepływu przez model, ślad aerodynamiczny i warstwę przyścienną na ściankach przestrzeni pomiarowej powodują znaczne błędy mierzonych wielkości. Uwzględniając konstrukcję tunelu oraz wynikające stąd ograniczenia przedstawiono różne sposoby zminimalizowania tych niepożądanych efektów. Wykorzystując symulacje numeryczną przedstawiono rozkłady ciśnień wzdłuż ścianki górnej i dolnej przestrzeni pomiarowej oraz rozkłady współczynnika ciśnienia na profilu dla różnych konfiguracji. Dla przestrzeni pomiarowej z rozbieżnymi ściankami uzyskano zadawalające wyniki, zbieżne z wynikami dla opływu w przestrzeni swobodnej.